

RSC Advances



This is an *Accepted Manuscript*, which has been through the Royal Society of Chemistry peer review process and has been accepted for publication.

Accepted Manuscripts are published online shortly after acceptance, before technical editing, formatting and proof reading. Using this free service, authors can make their results available to the community, in citable form, before we publish the edited article. This *Accepted Manuscript* will be replaced by the edited, formatted and paginated article as soon as this is available.

You can find more information about *Accepted Manuscripts* in the [Information for Authors](#).

Please note that technical editing may introduce minor changes to the text and/or graphics, which may alter content. The journal's standard [Terms & Conditions](#) and the [Ethical guidelines](#) still apply. In no event shall the Royal Society of Chemistry be held responsible for any errors or omissions in this *Accepted Manuscript* or any consequences arising from the use of any information it contains.

.Synthesis, structure and luminescence characteristics of a novel red phosphor $\text{NaLa}_9(\text{GeO}_4)_6\text{O}_2:\text{Eu}^{3+}$ for light emitting diodes and field emission displays

Yaxin Cao, Ge Zhu and Yuhua Wang

Key Laboratory for Special Function Materials and Structural Design of the Ministry of Education,
School of Physical Science and Technology, Lanzhou University, Lanzhou, 730000, China.

E-mail: wyh@lzu.edu.cn; Fax: +86-931-8913554; Tel: +86-931-8912772

Abstract: In order to explore a new kind of red phosphor for near ultraviolet white light emitting diodes (NUV-WLEDs) and field emission displays (FEDs), Eu^{3+} doped $\text{NaLa}_9(\text{GeO}_4)_6\text{O}_2$ was synthesized and its structure and luminescence properties were studied for the first time for fundamental research. The results indicated that they are all crystallized in hexagonal crystal system with the $P63/m$ space group. Eu^{3+} doped $\text{NaLa}_9(\text{GeO}_4)_6\text{O}_2$ with the content of 0.07 has optimal photoluminescence properties, which had a dominant red emission peak at 612 nm (${}^5\text{D}_0\text{-}{}^7\text{F}_2$) with CIE coordinates of (0.6444, 0.3544) under 392 nm excitation and the quantum efficiency of 45.2%. Additionally, the thermal quenching property has been studied and its possible mechanism has also been expounded. Furthermore, the cathodoluminescence (CL) property was investigated and the result revealed that the sample had excellent degradation property for FEDs. The study reveals that $\text{NaLa}_9(\text{GeO}_4)_6\text{O}_2.0.07\text{Eu}^{3+}$ could be a suitable red-emitting phosphor candidate for NUV-WLEDs and FEDs.

Keywords: NUV-WLED, FED, phosphor

1. Introduction

Over the past few years, white light emitting diodes (WLEDs) has become an interesting field for many excellent characteristics, such as high efficiency, long lifetime, reliability, toxicity-free and energy-saving, etc.¹⁻³ In recent years, LED technology has attracted much attention as a potential replacement for incandescent light sources.^{4,5} LEDs used for lighting are always formed with LED chips and one or several kinds of phosphors. By far, the common used chips include blue LED chips and near ultraviolet

(NUV) LED chips while desirable LED phosphors must possess strong absorption in the region of the LED chips emission, high luminescence efficiency, excellent chemical and stability, low-cost and environmental friendliness.⁶ Conventional methods for generating white light using LEDs involve blending light from a blue LED chip with appropriate quantities of a yellow-emitting phosphor, such as cerium-doped yttrium aluminum garnet (YAG:Ce³⁺), on top of the blue LED chip.^{3,7,8} When the chip is driven under certain current, blue light is emitted by the InGaN chip through electron-hole recombination in the p-n junctions while some of it excites the YAG:Ce³⁺ phosphor to emit yellow light, and then the rest of the blue light would mix with the yellow light to generate white light. However, it suffers weakness of poor color rendering index (Ra < 80) because of the lack of red-light contribution, causing high color temperature.⁹⁻¹³ An alternative approach is to use an ultraviolet (UV)-LED to stimulate red-, green-, and blue-emitting (RGB) phosphors and NUV-LED chips could be more attractive. It might conquer the aforementioned pitfalls of the blue LED chip and on the other hand, NUV-LEDs are optically much more stable. It is considered that UV-LEDs might predominate solid-state-lighting (SSL) development for their high efficiency and easy fabrication.¹⁰ Until now, The blue and green phosphors, such as Ca₅(PO₄)₃Cl:Eu²⁺, BaMgAl₁₄O₂₃:Eu²⁺/Mn²⁺, BaMgAl₁₀O₁₇:Eu²⁺/Mn²⁺, etc. are commercially available and could meet the requirements of NUV excitation in terms of spectra. However, we are suffering from lack of identified red phosphors for NUV-WLED application. There have been some reports on nitride-based and sulfide red phosphors, but Ce³⁺-, Eu²⁺-, or Mn²⁺-doped sulfide phosphors, however, suffer the problems of absorption of visible light and poor stability when exposed to air and high temperature. Additionally, it is also challengeable to make the nitride-based phosphors apply in industrialization for phosphor converted (pc)-WLEDs because the reported nitride based red phosphors will absorb not only the NUV lights but also the blue-green lights and they are excluded here because the absorption of visible light would decrease the total luminous efficiency.^{14,15} Therefore, much more effort is required to develop red phosphors. In this regard, researchers had paid more attention to oxide-based phosphors and some further research had been done to improve the luminescence properties, for example, using ligand

passivant.¹⁶ Moreover, the FED is a promising candidate for the next generation of information display.¹⁷ For the realization of the full color FED, extensive research has been conducted to find new and more suitable FED phosphors. Standard sulfide phosphors, which have been studied for use in FED, however, are unstable under electron-beam bombardment, resulting in a chemical degradation of phosphor layer.^{18,19} In this respect, nonsulfide phosphors are desired in FED applications for improved stability, and many oxide phosphors have been investigated to escape the obstacles associated with degradation of sulfide phosphors.²⁰⁻²² So it is also indispensable to search for phosphors that possess appropriate properties for FEDs.

Continuous attention has been paid to the discovery of rare-earth-activated silicate phosphors in a long run and recently, germanate phosphors has also been focused on, such as $\text{Mg}_3\text{Y}_2\text{Ge}_3\text{O}_{12}:\text{Ce}^{3+}$ and $\text{Mg}(\text{F})\text{GeO}_6:\text{Mn}^{2+}$.²³ This is because Si and Ge elements are in the same fourth main group, namely, their outer electronic distributions are same. Their compound should be in the form of similar crystal structure and result in similar physical and chemical properties. Meanwhile, the difference of the electronegativities of Ge and O ($\Delta X = 1.43$) is close to that of Si and O ($\Delta X = 1.54$), so rare earth doped germanates could also have excellent optical properties.²⁴ Among numerous of rare earth ions, Eu^{3+} was usually chosen as a typical and efficient activator for red emitting phosphor and its photoluminescence emission strongly depends on the symmetry of the crystal structure of the Eu^{3+} -occupied site in the host. The optical transitions of Eu^{3+} ions originating from the electronic dipole and magnetic dipole interactions of the internal 4f electrons are affected by crystal environment seriously. If the Eu^{3+} ions occupy sites with inversion symmetry, emission peaks in the range of 590-600 nm from the $^5\text{D}_0$ - $^7\text{F}_1$ magnetic-dipole transition will dominate the emission, which is not affected much by the site symmetry. On the contrary, the emission peaks around 610-630 nm from the $^5\text{D}_0$ - $^7\text{F}_2$ electronic dipole transition will dominate the emission if the Eu^{3+} ion substitutes a site with no inversion symmetry and this part will be notably affected by local asymmetry environment.^{25,26} However, the parity-forbidden nature of Eu^{3+} results in weak absorption cross section and thus low external quantum efficiency. There is one potential way to overcome this, to enhance the Eu^{3+} doping concentration. But it makes

sense before the quenching concentration only.^{27,28} So it is necessary to find out the right concentration to obtain the optimal photoluminescence.

It is well known that apatite-type compounds have good luminescent properties. The luminescent properties of $M^+Ln_9(SiO_4)_6O_2$ ($M^+=Li, Na$) and $M_2^{2+}Ln_8(SiO_4)_6O_2$ ($M^{2+}=Mg, Ca$) activated by Eu^{3+} have been discussed by Blasse.²⁹ According to report by Takahashi, an important structural characteristic of $NaLa_9Ge_6O_{26}$ is that the La-La distances are quite large, i.e., 0.364 nm on nearest-neighbor sites and 0.40324(7) nm on the next-nearest neighbor sites.³⁰ This fact elicits interest in the potential luminescent properties of this material, especially with respect to the phenomenon of concentration quenching. In this paper, the synthesis and crystal structure of ~~a new germanate~~ $NaLa_9(GeO_4)_6O_2$ which has a typical structure of apatite is investigated and the luminescence properties of the Eu^{3+} doped $NaLa_9(GeO_4)_6O_2$ are studied for the first time. The photoluminescence and cathodoluminescence properties of the Eu^{3+} doped $NaLa_9(GeO_4)_6O_2$ are investigated which have shown that $NaLa_9(GeO_4)_6O_2:Eu^{3+}$ could be a potential red-emitting phosphor for NUV-WLEDs and FEDs.

2. Experimental

2.1 Materials and synthesis

Samples of Eu^{3+} doped $NaLa_9(GeO_4)_6O_2$ were synthesized using a traditional solid-state reaction. Analytical reagents (AR) Na_2CO_3 , La_2O_3 , Eu_2O_3 and GeO_2 (99.99%) were used as the starting materials. Stoichiometric amounts of the starting materials were firstly mixed into an agate mortar and ground substantially. Then the raw materials were put into a crucible and heated by a box-type furnace in air. The samples were firstly heated to 800 °C for 2 hours, and then further heated to 1380 °C for 5 hours, finally, the samples cooled slowly to room temperature.

2.2 Characterization

The crystal structure was identified using a Bruker D2 PHASER X-ray Diffractometer (XRD) with graphite monochromator using Cu $K\alpha$ radiation ($\lambda = 1.54056 \text{ \AA}$), operating at 30 kV and 15 mA and Fourier transform infrared spectroscopy (FTIR, Nicolet NEXUS 670). Reflectance spectra were measured on PE lambda950 UV-vis spectrophotometer using the $BaSO_4$ white powder as the reference. The

photoluminescence (PL) and photoluminescence excitation (PLE) spectra were obtained using a FLS-920T fluorescence spectrophotometer (Edinburgh Instruments) equipped with a 450 W Xe light source and double excitation monochromators. The PL decay curves were measured using an FLS-920T fluorescence spectrophotometer with an F900 nanosecond flash hydrogen lamp as the light source. High temperature luminescence intensity measurements were carried out using an aluminum plaque with cartridge heaters; the temperature was measured by thermocouples inside the plaque and controlled with a standard TAP-02 high temperature fluorescence controller (Orient KOJI instrument Co., Ltd.). The CL properties of the samples were obtained using a modified Mp-Micro-S instrument (Horiba Jobin Yvon).

3. Results and discussion

3.1 Study on phase identification and crystal structure

A series of different concentration of Eu^{3+} doped $\text{NaLa}_9(\text{GeO}_4)_6\text{O}_2 \cdot x\text{Eu}^{3+}$ ($0 \leq x \leq 0.11$) have been synthesized. The XRD results were shown in Fig. 1a. It indicates that the peaks have a shift to a higher angle area when increase the concentration of Eu^{3+} ion. The radius of six-, seven-, nine-fold coordinated Eu^{3+} is 0.947 Å, 1.01 Å and 1.120 Å, respectively while the radius of six-, seven-, nine-fold coordinated La^{3+} is 1.032 Å, 1.10 Å and 1.216 Å, respectively.³¹ According to Bragg equation ($2d\sin\theta = \lambda$), when Eu^{3+} substitutes La^{3+} in the crystal site, it could cause a lattice distortion which will make a smaller d and a larger θ should express due to this. The experimental result fit Wegener's rules well and it also indicated that Eu^{3+} ion has been embedded in the host lattice well.

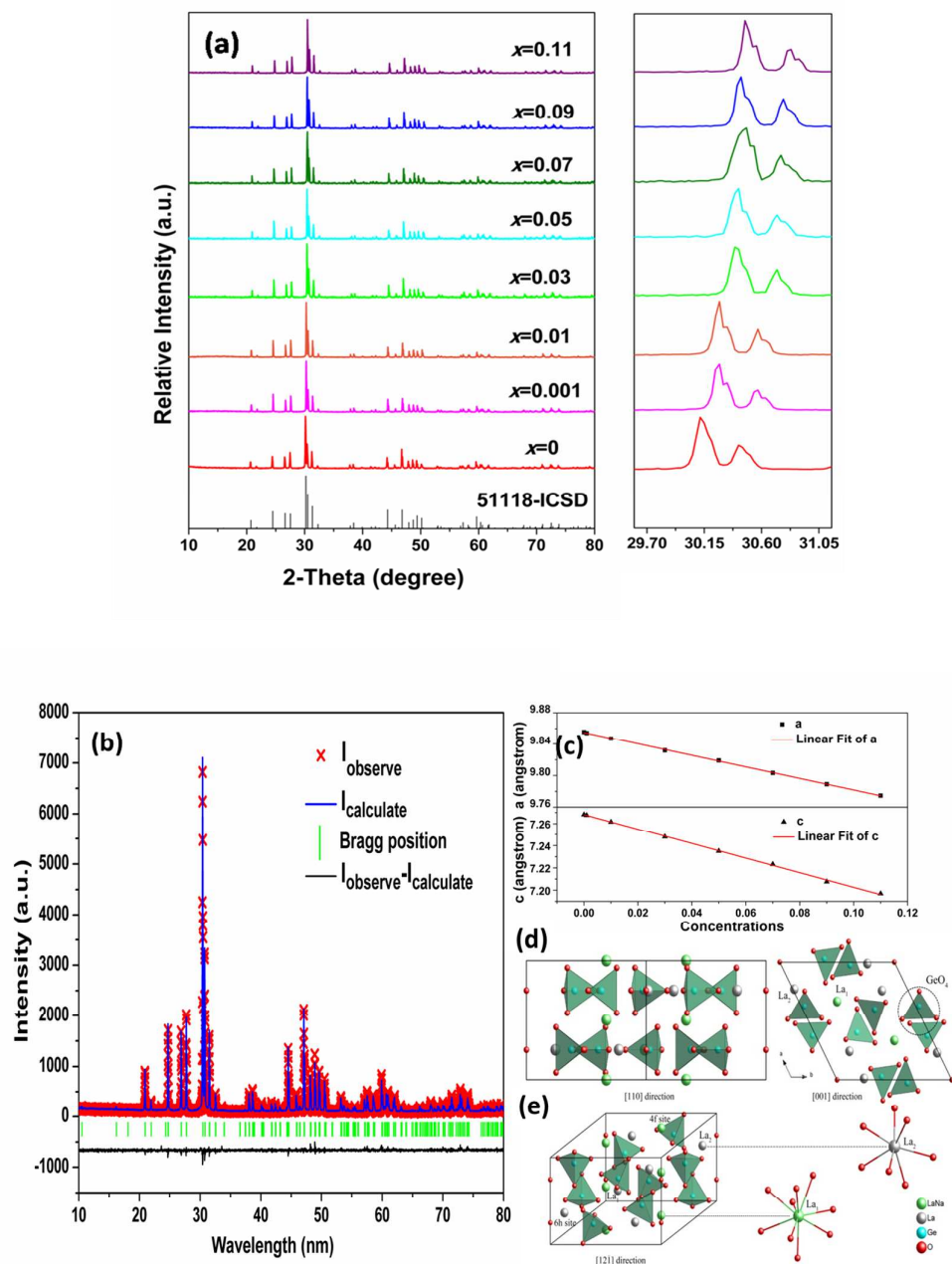


Fig. 1 (a) XRD patterns of different concentrations of Eu^{3+} doped samples, the right part shows patterns from 29.6 to 31.15 degree in detail; (b) XRD refinement result of $\text{NaLa}_9(\text{GeO}_4)_6\text{O}_2:0.07\text{Eu}^{3+}$; (c) The different lattice parameters as a function of Eu^{3+} concentrations; (d) the structural views of $\text{NaLa}_9(\text{GeO}_4)_6\text{O}_2:0.07\text{Eu}^{3+}$ along [110], [001] direction, respectively and (e) a structural view of $\text{NaLa}_9(\text{GeO}_4)_6\text{O}_2:0.07\text{Eu}^{3+}$ in the direction of [12T] and coordination environments for all independent metal atoms in $\text{NaLa}_9(\text{GeO}_4)_6\text{O}_2:0.07\text{Eu}^{3+}$.

Figure 1b shows structural refinements of the XRD patterns of $\text{NaLa}_9(\text{GeO}_4)_6\text{O}_2:0.07\text{Eu}^{3+}$ compound as a typical sample. The pink crosses and blue

solid lines depict the observed and calculated patterns, respectively. The green short vertical lines show the position of Bragg reflections of the calculated patterns. The difference between the experimental and calculated patterns is plotted by black line at the bottom. The structure parameters reported on $\text{NaLa}_9(\text{GeO}_4)_6\text{O}_2$ were used as initial parameters in the Rietveld analysis.³² The refined results of $\text{NaLa}_9(\text{GeO}_4)_6\text{O}_2$ are summarized in Table 1. The residual factors are $R_{\text{wp}} = 8.15\%$, and $R_p = 6.19\%$. The results indicate that the powder sample is crystallized in hexagonal symmetry with space group P63/m. The lattice parameters of $\text{NaLa}_9(\text{GeO}_4)_6\text{O}_2:0.07\text{Eu}^{3+}$ are $a = 9.862(0) \text{ \AA}$ and $c = 7.234(5) \text{ \AA}$, respectively. Furthermore, the lattice parameters of different concentration of Eu^{3+} doped samples were calculated and the relationship between concentration and parameters were shown in Fig. 1c. These results indicated that the lattice parameters decreased with increasing Eu^{3+} concentration with a linear relation. This is because when Eu^{3+} is doped, the host lattice would have a contraction due to its smaller ionic radius, and the more Eu^{3+} is doped, the severer the contraction would be.

Table 1. The refined unit cell parameters and residual factors.

<i>Atom</i>	<i>Ox.</i>	<i>Wyck.</i>	<i>Site</i>	<i>S.O.F.</i>	<i>x/a</i>	<i>y/b</i>	<i>z/c</i>	<i>occupancy</i>	<i>U_{eq}</i>
La1	3	4f	3..	0.75	1/3	2/3	0.0003(2)	0.65779	0.01629
Na1	1	4f	3..	0.25	1/3	2/3	0.0003(2)	0.65779	0.01629
La2	3	6h	m..		0.24157(4)	0.01251(4)	1/4	0.68608	0.01612
Ge1	4	6h	m..		0.37346(7)	0.40143(7)	1/4	0.63709	0.01299
O1	-2	6h	m..		0.4867(6)	0.3121(6)	1/4	0.88605	0.12412
O2	-2	6h	m..		0.5234(6)	0.3961(5)	3/4	1.00000	0.13668
O3	-2	12i	1		0.2468(4)	0.3407(6)	0.4396(5)	0.88037	0.08165
O4	-2	2a	-6..		0	0	1/4	0.78662	0.05385

According to the refinement results, in $\text{NaLa}_9(\text{GeO}_4)_6\text{O}_2$ structure, there are 42 crystallographically independent atoms in the unit cell, including 1 Na, 9 La, 6 Ge and 26 O atoms. Figure 1d shows the projections of the structures of $\text{NaLa}_9(\text{GeO}_4)_6\text{O}_2$ along [110] and [001] directions. As shown in Fig. 1e, the crystal structure of $\text{NaLa}_9(\text{GeO}_4)_6\text{O}_2$ is a three-dimensional framework consisting of LaO_7 , LaO_9 , GeO_4 and NaO_9 polyhedra. In order to afford clear views of the structure, only GeO_4 (dark green part) is presented as polyhedron in Fig. 1d and 1e. The view from [001] direction clearly shows that the

GeO₄ tetrahedra form polyhedra rings around the c-axis to form layers stacking induces tunnels parallel to the c-axis with large cavities in which the La or Na atoms are located, with seven and nine coordinations. Fig. 1e clearly shows the coordination environment of La (including La1 and La2) and Na (the same as La1) atoms in NaLa₉(GeO₄)₆O₂. La1 (Na) in the 4f site coordinated with nine O atoms of which the O atoms are from GeO₄ tetrahedra only. La2 in the 6h site coordinated with seven O atoms including six from GeO₄ tetrahedra and one in the tunnel. The two different La positions of La1 and La2 are located in GeO₄ coordination polyhedra. Based on the effective ionic radius and the similar electric charge, when Eu³⁺ enter into the lattice matrix, they are expected to randomly enter into La³⁺ sites and experience specific local asymmetry environment, that is, the La1 site and La2 site, both are inversion symmetry sites.

The FTIR spectrum of the as-prepared material is shown in Fig. 2a. The absorption at 3433.3 cm⁻¹ and 1628.2 cm⁻¹ can be attributed to O-H vibrations (stretching and bending, respectively) of the adsorbed water on the surface of the phosphors. It also displays several characteristic absorptions around 746.4, 477.1 cm⁻¹ which attributed to Ge-O vibration.³³

Diffuse reflectance spectra (DRS) of the matrix and 0.03 Eu³⁺ doped samples are shown in Fig. 2b. A broad band was observed in the spectrum of the matrix before 350 nm. For the 0.03 Eu³⁺ doped sample, the broad band can be attributed to Eu³⁺-O²⁻ charge transition (CT) and two small peaks at 392 and 462 nm were related to ⁷F₀-⁵L₆ and ⁷F₀-⁵D₂ transition, respectively. These optical absorptions are due to the excitation of electrons from valence band (VB) to conductive band (CB). Although an exact discussion of transitions from VB to CB requires calculation of the excited state electronic structure, the calculated static electronic band, as an approximation, may still provide important information. The calculated band structure shown in Fig. 3 revealed that NaLa₉(GeO₄)₆O₂:Eu is a direct band gap material. The calculated direct band gap E_g is 3.54 eV. The band gap can be also calculated by the Kubelka-Munk equation.³⁴

$$F(R_{\infty}) = (1 - R_{\infty})^{1/2} / 2R_{\infty} = k/s \quad (1)$$

where R_∞ is the diffuse reflectance of the layer relative to standard, k is the molar absorption coefficient of the sample and s is the scattering coefficient. According to the

relationship between diffuse reflectance R_∞ and energy E shown in the inset diagram in Fig. 2b, the $F(R_\infty)$ as a function of E can be obtained, and the intersection between the linear fit of $F(R_\infty)$ and the photon energy (wavelength) axis gives the value of the band gap.³⁵ The band gap of $\text{NaLa}_9(\text{GeO}_4)_6\text{O}_2$ was determined to be 3.11 eV (398 nm) through the $F(R_\infty)$ -energy relation graph. The calculated band gap values are similar through the two methods. The inconsistency comes mainly from errors of correlation function calculations, and slightly from the errors introduced from the measurement of the DRS and the estimation by using equation 1.

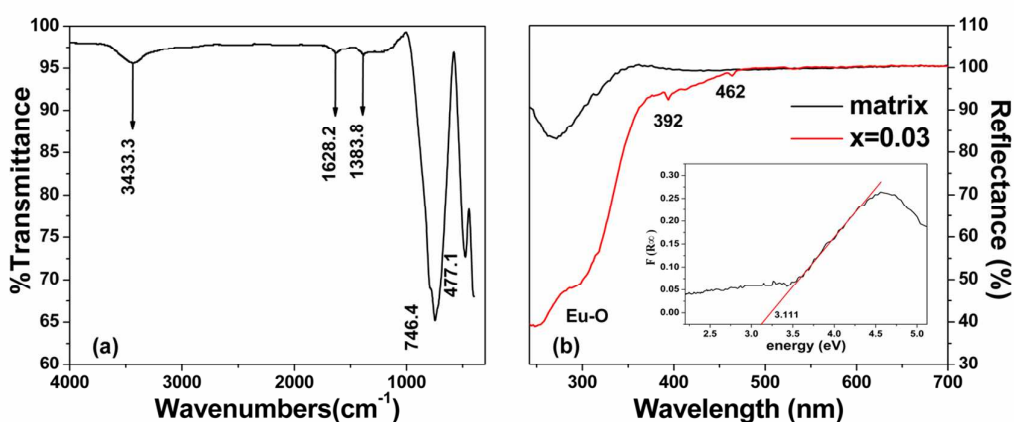


Fig. 2 (a) FTIR spectrum of $\text{NaLa}_9(\text{GeO}_4)_6\text{O}_2$, and (b) DRS of the matrix and $\text{NaLa}_9(\text{GeO}_4)_6\text{O}_2:0.07\text{Eu}^{3+}$, the inset shows the determined band gap of $\text{NaLa}_9(\text{GeO}_4)_6\text{O}_2$ being 3.11 eV.

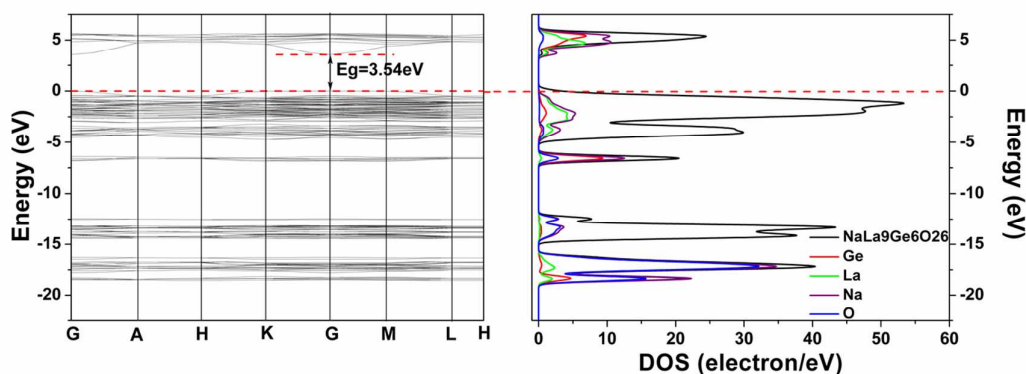


Fig. 3 Calculated band structures (left) and DOS (right) of hexagonal $\text{NaLa}_9(\text{GeO}_4)_6\text{O}_2$ near the Fermi energy level (the red dash below). The Fermi energy is the zero of the energy scale. E_g is the calculated forbidden band gap of the ground state of the system.

3.2 Photoluminescence properties of Eu³⁺ doped NaLa₉(GeO₄)₆O₂

The PLE spectra of NaLa₉(GeO₄)₆O₂:*x*Eu (0.001 ≤ *x* ≤ 0.11) samples monitoring at 612 nm shown in Fig. 4a consists of a broad band centered at around 300 nm and several sharp peaks ranging from 350 to 500 nm. The band excitation can be assigned to the charge transition band (CTB), resulting from an electron transfer from the ligand O²⁻ (2P⁶) orbital to the empty state of 4f⁶ in the Eu³⁺ ion (Eu³⁺-O²⁻) and it contains a small peak at 317 nm that corresponded to ⁷F₀-⁵H_J transition. The latter line peaks should relate to the characteristic 4f-4f transitions of Eu³⁺ ions; those correspond to the transitions from the ground state ⁷F₀ to the excited levels ⁵D₄ (361 nm), ⁵L₇, ⁵G_J (375 nm, 380 nm), ⁵L₆ (392 nm), ⁵D₃ (412 nm) and ⁵D₂ (462 nm) of Eu³⁺. Phosphors for NUV-LEDs should have strong absorption around 400 nm (emission wavelength of NUV-LED chips). Obviously, the PLE spectra shows strong absorption around 400 nm (392 nm), indicating that the phosphor can be a candidate for red-emitting phosphors for NUV-LEDs.

Fig. 4b shows the emission spectra of the series phosphors under 392nm excitation. The spectra consists of a number of sharp lines mainly ranging from 450 to 750 nm, which peaked at 578 nm (⁵D₀-⁷F₀), 588 nm (⁵D₀-⁷F₁), 612 nm (⁵D₀-⁷F₂), 650 nm (⁵D₀-⁷F₃) and 701 nm (⁵D₀-⁷F₄), respectively. The inset shows the transitions from higher ⁵D₁ state, peaking at 535 nm (⁵D₁-⁷F₁) and 553 nm (⁵D₁-⁷F₂). The line shape of the emission almost does not change with the variation of Eu³⁺ concentration because most of the valence electrons of trivalent rare-earth elements are shielded by 5s and 5p outer electrons, and the f-f transitions of trivalent lanthanides are weakly affected by ligand ions in the crystals.³ For Eu³⁺, the relative intensity of ⁵D₀-⁷F_J multiplet emission is also an important factor that determines the chromaticity or saturation of red color; in general, the larger the magnitude of ((⁵D₀-⁷F₂)/ (⁵D₀-⁷F₁)) (*R/O*), the closer to the optimal value of the color chromaticity. On the other hand, *R/O* ratio can also perform as the asymmetry ratio, which suggests the degree of distortion.^{36,37} In this study, we observed that the *R/O* ratio increased with increasing *x* value. As shown in Fig. 4c, the asymmetry ratio increased as the concentration of Eu³⁺ ions increased. This is because when Eu³⁺ ions were doped, it could cause distortion of the host lattice and the more Eu³⁺ ions are,

the fiercer would the distortion be. The intensity of transition ${}^5D_0-{}^7F_2$ would be more sensitive to the coming distortion than ${}^5D_0-{}^7F_1$, as a result, the R/O ratio increased. The PL intensity was found to increase with increasing Eu^{3+} concentration before 0.07, and after that, intensity decrease for a concentration of doped Eu^{3+} greater than 0.07, which is attributed to a concentration-quenching effect as shown in Fig. 4a and Fig. 4b. The comparison of PL property between commercial phosphor $\text{Y}_2\text{O}_3:\text{Eu}^{3+}$ and synthesized $\text{NaLa}_9(\text{GeO}_4)_6\text{O}_2:0.07\text{Eu}^{3+}$ in Fig. 4d shows that the latter has broader emission lines which results in a larger integral area, which indicates that the synthesized $\text{NaLa}_9(\text{GeO}_4)_6\text{O}_2:0.07\text{Eu}^{3+}$ have a higher brightness than the commercial phosphor. It is well known that quantum efficiency is very important when it comes to real application. Normally, Eu^{3+} shows relatively high internal quantum efficiency in solids at low concentration. The higher concentration could give a higher external quantum efficiency but quench the Eu^{3+} PL in $\text{NaLa}_9(\text{GeO}_4)_6\text{O}_2$.^{38,39} We measured the quantum efficiency of $\text{NaLa}_9(\text{GeO}_4)_6\text{O}_2:0.07\text{Eu}^{3+}$ which has the heaviest doping amount but doesn't quench to be 45.2%.

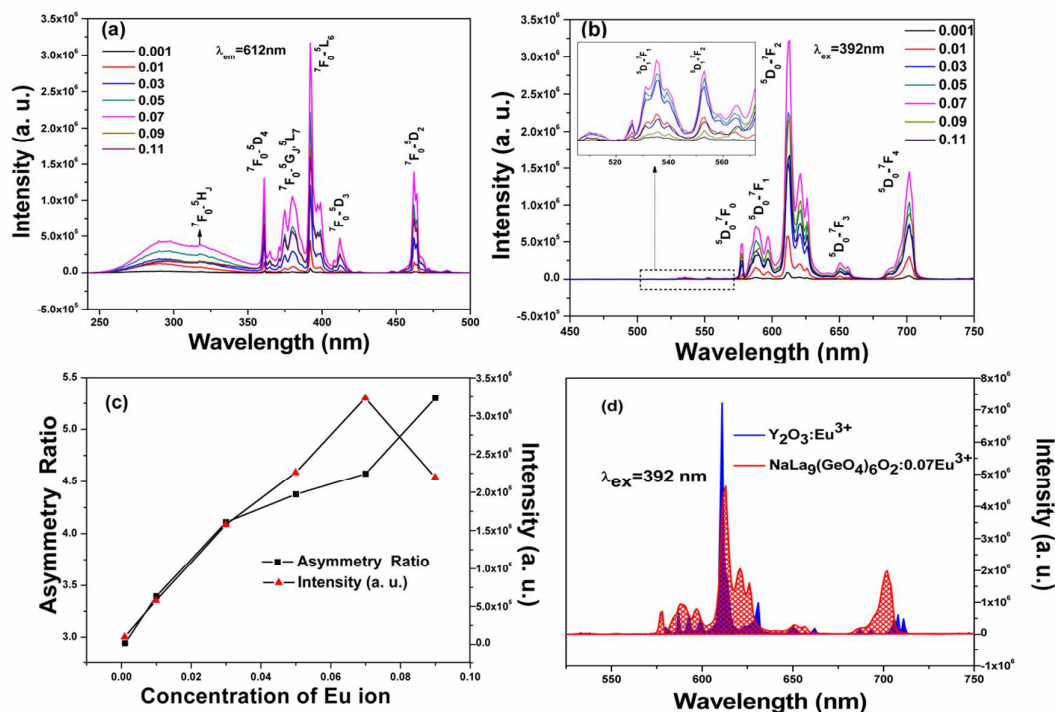
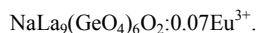


Fig. 4 (a) The PLE spectra of samples with Eu^{3+} concentrations from 0.001 to 0.11; (b) PL spectra of all the samples

(the inset shows the magnified part reveals the transitions from higher 5D_1 energy); (c) diagram of concentration affected asymmetry ratio and relative intensity and (d) photoluminescence comparison of commercial phosphor and



The temperature stability of optical properties is important for evaluating luminescent materials, since the luminescent materials may suffer from high temperature during long-term operation.⁴⁰ Fig. 5a shows the luminescence intensity of $\text{NaLa}_9(\text{GeO}_4)_6\text{O}_2:0.07\text{Eu}^{3+}$ at different temperature when excited at 392 nm. It indicated that the PL intensity decreased with the increasing temperature in an approximate liner manner (shown in the inset of Fig. 5a) which reveals that the phosphor may have potential to be used for a temperature sensor. The luminescence thermal quenching effect is usually attributed to the nonradiative relaxation through the crossing point between the excited state and the ground state in the configurational coordinate diagram.⁴¹ Fig. 5b shows the possible mechanism of thermal quenching. When there is irradiation, electrons on the ground state would be excited to the excited states and then emits photons while back to the ground state. Firstly, electrons are excited to 5D_0 and 5D_1 states. Generally, the electrons on 5D_1 state can cross-relaxing to the 5D_0 state and then the electrons could return to the ground states through pathway of the thermal quenching which is related to the 5D_0 state and $\text{Eu}^{3+}-\text{O}^{2-}$ CTB: some electrons overcome the activation energy ΔE assisted by phonons as the temperature increases and then feed to the 7F_J state, which provides the nonradiative process (via ③), and on the other hand, the remaining electrons contribute to the 5D_0 - 7F_2 emission at 612 nm (via ①). A few of the electrons excited to 5D_1 state return to the ground state directly which cause the emission 5D_1 - 7F_J ($J=1, 2$) (via ②), the emission were very weak due to the small transition odds.

The nonradiative transition probability is strongly dependent on temperature resulting in the decrease of emission intensity. The temperature dependence of the emission intensities of phosphors could be described according to the following modified Arrhenius equation:³⁷

$$I(T) = I_0 [1 + A \exp(-\Delta E/kT)]^{-1} \quad (2)$$

Where $I(T)$ is the intensity at a given temperature, I_0 is the initial intensity, k is the

Boltzmann constant, T is the temperature, and ΔE is the activation energy from the 5D_0 state to the CTB and can be regarded as a constant because the shape of the emission curve did not change significantly. Based on equation 2, we can plot $\ln [(I_0/I) - 1]$ vs. $1/kT$ yielding a straight line, and the activation energy ΔE is obtained from the slope of the plot. As shown in Fig. 5c, the experimentally calculated activation energy ΔE was 0.279 eV for $\text{NaLa}_9(\text{GeO}_4)_6\text{O}_2:0.07\text{Eu}^{3+}$.

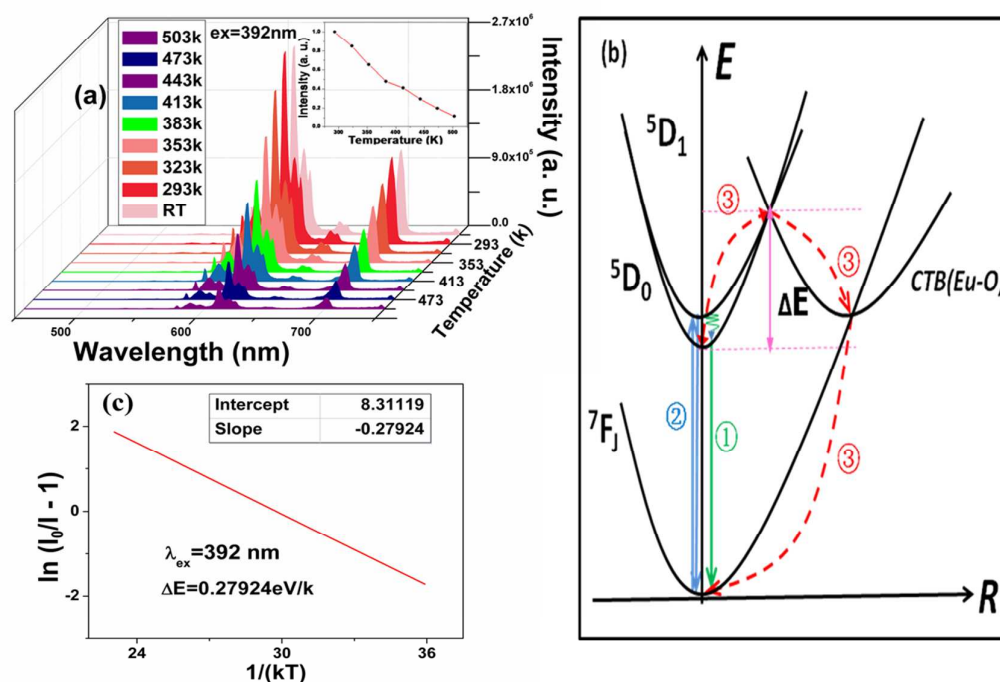


Fig. 5 (a) The temperature dependent emission spectra of the $\text{NaLa}_9(\text{GeO}_4)_6\text{O}_2:0.07\text{Eu}^{3+}$ phosphor. The inset shows temperature dependent peak values of the sample; (b) the schematic illustration of a configurational coordinate diagram of the thermal quenching process in Eu^{3+} doped $\text{NaLa}_9(\text{GeO}_4)_6\text{O}_2$ and (c) the calculated activation energy for thermal quenching of the $\text{NaLa}_9(\text{GeO}_4)_6\text{O}_2:0.07\text{Eu}^{3+}$ phosphor.

Fig. 6a shows the luminescence decay curves of the phosphor $\text{NaLa}_9(\text{GeO}_4)_6\text{O}_2:x\text{Eu}^{3+}$ excited at 392 nm and monitored at 612 nm. All the curves can be well fitted by an exponential function and the lifetime value can be given to the average lifetime defined as:^{43,44}

$$\tau_{\text{average}} = \int tI(t)dt / \int I(t)dt \quad (3)$$

For 5D_0 - 7F_2 (612 nm) of Eu^{3+} ions, the lifetimes vary from 1.316 to 1.438 ms for

different concentrations. The lifetime becomes shorter gradually when increasing the concentration of Eu^{3+} . For ${}^5\text{D}_1$ - ${}^7\text{F}_1$ (553 nm), ${}^5\text{D}_0$ - ${}^7\text{F}_1$ (588 nm), ${}^5\text{D}_0$ - ${}^7\text{F}_2$ (612 nm) and ${}^5\text{D}_0$ - ${}^7\text{F}_4$ (701 nm), the average lifetimes are 0.716, 1.387, 1.328 and 1.379 ms, respectively, which is shown in Fig. 6b. From the lifetimes, it can be found that the lifetime of the higher energy level (${}^5\text{D}_1$) emission is shorter than that of the lower energy (${}^5\text{D}_0$) emission. This is because the higher energy level is more metastable than the lower energy level, and the electron at the higher energy level would like to either transition to the ground (${}^7\text{F}_J$, $J = 1, 2, 3, 4$) state or relax to the low energy level nonradiatively by multiphonon emission.⁴⁵ Thus, the luminescence decay curve can also be used to distinguish the lower level ${}^5\text{D}_0$ with upper levels of Eu^{3+} , such as ${}^5\text{D}_1$, ${}^5\text{D}_2$ or ${}^5\text{D}_3$.

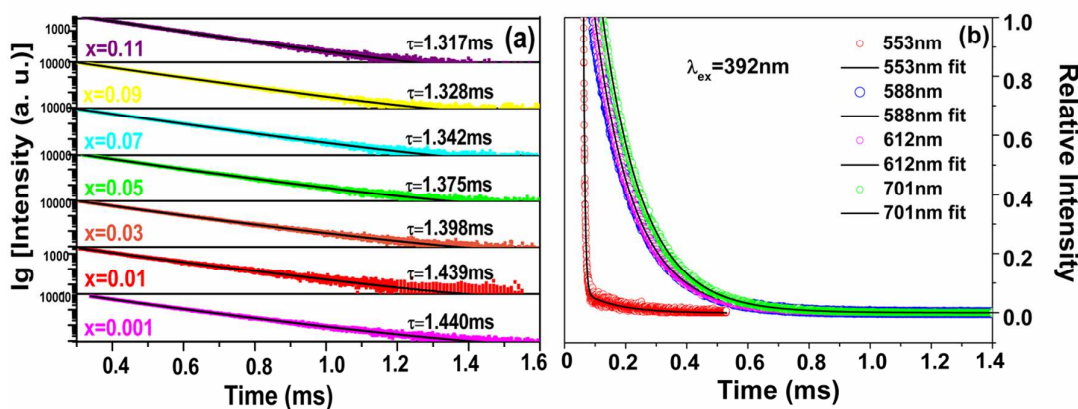


Fig. 6 (a) Decay curves of different concentrations of Eu^{3+} (from 0.001 to 0.11) doped samples when excited at 392 nm and (b) 0.07 Eu^{3+} doped sample monitoring under different wavelength of 553, 588, 612, 701 nm when excited at 392 nm.

3.3 Cathodoluminescence properties of Eu^{3+} ions in $\text{NaLa}_9(\text{GeO}_4)_6\text{O}_2$

The CL properties of the sample $\text{NaLa}_9(\text{GeO}_4)_6\text{O}_2:0.07\text{Eu}^{3+}$ have been investigated to explore their potentials in the development of efficient red phosphors for FED systems. For cathodoluminescence, the Eu^{3+} ions are excited by the plasma produced by the incident electrons. The CL spectrum of $\text{NaLa}_9(\text{GeO}_4)_6\text{O}_2:0.07\text{Eu}^{3+}$ consists of several characteristic emission lines of Eu^{3+} , peaking at 536 nm, 557 nm, 591 nm, 615 nm, 655 nm and 705 nm, respectively. Compared with its PL spectra, the prominent emission becomes broader and exhibits a little red shift of 1~4 nm. This phenomenon may due to

the energy level structures of vacancy defects and a different excitation mechanism.⁴⁶ The CL emission intensities for the samples $\text{NaLa}_9(\text{GeO}_4)_6\text{O}_2:0.07\text{Eu}^{3+}$ have been investigated as a function of accelerating voltage and filament current, respectively, which are shown in Fig. 7a and 7b, respectively. When the filament current was given as 80 mA, the CL intensity gradually increased with applied voltage from 3.0 to 10.0 kV (Fig. 7a). And when it was excited under a voltage of 8.0 kV, the CL intensity also increased with increasing of the filament current from 10 to 100 mA (Fig. 7b). It can be interpreted that with the increase of accelerating voltage or filament current, more plasma was produced, which resulted in more ions being excited and thus the CL intensity increased.⁴⁷ The increase in CL brightness with an increase in the electron energy and filament current is attributed to the deeper penetration of the electrons into the phosphor body and the larger electron beam current density.^{47,48}

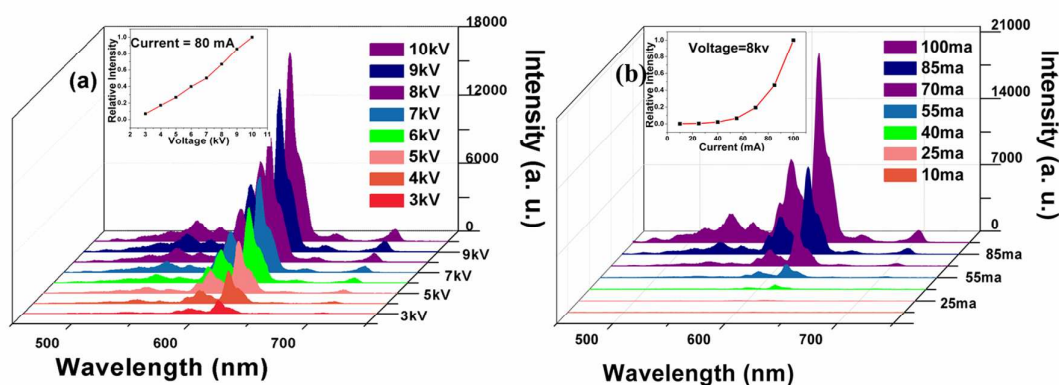


Fig.7 Cathodoluminescence properties of $\text{NaLa}_9(\text{GeO}_4)_6\text{O}_2:0.07\text{Eu}^{3+}$ (a) with a constant filament current 80 mA (the inset shows the voltage related CL intensity) and (b) under a constant voltage 8.0kV (the inset shows the current related CL intensity).

The degradation property of phosphors is very important for FED application. In general, the use of phosphors with poor efficiency at low voltage leads to the need for high current operation which enhances the phosphor degradation. And for most phosphors used in FEDs, the CL intensity decreased with the increase of the bombing times. This is because during continuous electron bombardment, graphitic carbon will accumulate on the surface of phosphors and cause the well-known effect of carbon contamination, which will exacerbate surface charging, and thus lower the CL intensity.⁴⁹ Thus we tried to

investigate the degradation behavior of $\text{NaLa}_9(\text{GeO}_4)_6\text{O}_2:0.07\text{Eu}^{3+}$ sample under continuous low-voltage electron-beam excitation and this is showed in Fig. 8a. The accelerating voltage was kept at 8.0 kV and the filament current was 50 mA. As it shows that the CL intensity of $\text{NaLa}_9(\text{GeO}_4)_6\text{O}_2:0.07\text{Eu}^{3+}$ almost keep constant under a continuous electron bombardment which indicates that the synthesized phosphor could keep wonderful stability when used for FEDs. For comparison, the degradation property of the commercial $\text{Y}_2\text{O}_3:\text{Eu}^{3+}$ was also measured and their comparison result was shown in Fig. 8b. It is obvious that degradation property of the synthesized $\text{NaLa}_9(\text{GeO}_4)_6\text{O}_2:0.07\text{Eu}^{3+}$ is better than that of $\text{Y}_2\text{O}_3:\text{Eu}^{3+}$.

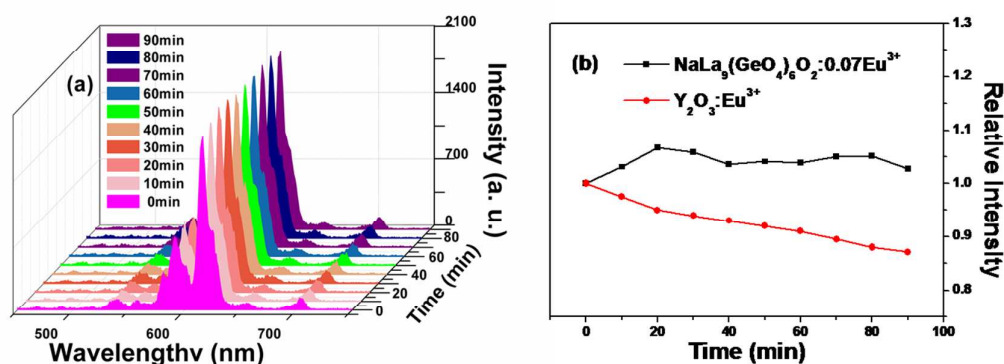


Fig. 8 (a) Degradation property of $\text{NaLa}_9(\text{GeO}_4)_6\text{O}_2:0.07\text{Eu}^{3+}$ and (b) time dependence intensity compared with $\text{Y}_2\text{O}_3:\text{Eu}^{3+}$.

Conclusion

In this work, a novel red-emitting phosphor $\text{NaLa}_9(\text{GeO}_4)_6\text{O}_2:x\text{Eu}$ has been successfully synthesized, while the structure and luminescence properties were investigated in detail. The results indicated that the sample $\text{NaLa}_9(\text{GeO}_4)_6\text{O}_2:0.07\text{Eu}^{3+}$ has optimal luminescence properties. Photoluminescence property of the synthesized $\text{NaLa}_9(\text{GeO}_4)_6\text{O}_2:0.07\text{Eu}^{3+}$ has been compared with $\text{Y}_2\text{O}_3:\text{Eu}^{3+}$ when under 392 nm excitation, which suggested that the former performs excellent lightness. It can be also found that $\text{NaLa}_9(\text{GeO}_4)_6\text{O}_2:0.07\text{Eu}^{3+}$ phosphor showed the bright red emission of Eu^{3+} $^5\text{D}_0$ - $^7\text{F}_2$ transitions and it performed an excellent degradation property under continuous low-voltage electron-beam excitation through its CL spectra. Therefore, the $\text{NaLa}_9(\text{GeO}_4)_6\text{O}_2:0.07\text{Eu}^{3+}$ with excellent photoluminescence and cathodoluminescence

could be a promising candidate for NUV-WLEDs and FEDs.

Acknowledgements

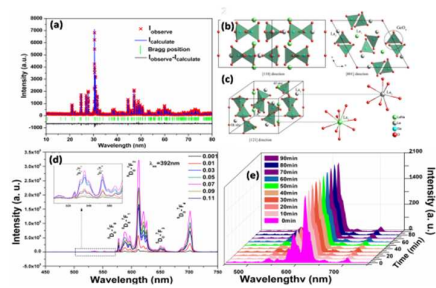
This work was supported by Specialized Research Fund for the Doctoral Program of Higher Education (No. 20120211130003) 35, the National Science Foundation for Distinguished Young Scholars (no. 50925206) and the National Development and Reform Commission.

References

1. E. F. Schubert and J. K. Kim, *Science*, 2005, **308**, 1274.
2. S. Nakamura, T. Mukai, and M. Senoh, *Appl. Phys. Lett.*, 1994, **64**, 1687.
3. S. Ye, F. Xiao, Y. X. Pan, Y. Y. Ma, and Q. Y. Zhang, *Mater. Sci. Eng. Rep.*, 2010, **71**, 1.
4. Y. Shimizu, K. Sakano, Y. Noguchi and T. Moriguchi, *U.S. Patent*, 1998, **998**, 925.
5. K. Sakuma, N. Hirotsuki, N. Kimura, M. Ohashi, R. J. Xie, Y. Yamamoto, T. Suehiro, K. Asano and D. Tanaka, *IEICE Trans. Electron*, 2005, **E88-C**, 2057.
6. X. Y. Huang, *Nature Photonics*, 2014, **8**, 748.
7. Hoppe and H. A. Angew, *Chem., Int. Ed.*, 2009, **48**, 3572.
8. C. Feldmann, T. Justel, C. R. Ronda and Schmidt, *P. J. Adv. Funct. Mater.*, 2003, **13**, 511.
9. D. A. Steigerwald, J. C. Bhat, D. Collins, R. M. Fletcher, M. O. Holcomb, M. J. Ludowise, P. S. Martin and S. L. Rudaz, *IEEE J. Sel. Top. Quant*, 2002, **8**, 310.
10. J. K. Sheu, S. J. Chang, C. H. Kuo, Y. K. Su, L. W. Wu, Y. C. Lin, W. C. Lai, J. M. Tsai, G. C. Chi and R. K. Wu, *IEEE Photonic Tech. Lett.*, 2003, **15**, 18.
11. M. S. Shur and A. Zukauskas, *Proc. IEEE*, 2005, **93**, 1691.
12. M. R. Krames, O. B. Shchekin, R. Mueller-Mach, G. O. Mueller, L. Zhou, G. Harbers and M. G. Craford, *J. Display Technol.*, 2007, **3**, 160.
13. Yamada, Y. Narukawa, H. Tamaki, Y. Murazaki and T. Mukai, *IEICE Trans. Electron*, 2005, **E88C**, 1860.
14. R. J. Xie and N. Hirotsuki, *Sci. Technol. Adv. Mater.*, 2007, **8**, 588.

15. X. H. He, N. Lian, J. H. Sun and M. Y. Guan, *J. Mater. Sci.*, 2009, **44**, 4763.
16. Q. L. Dai, M. E. Foley, C. J. Breshike, A. Lita, and G. F. Strouse, *J. Am. Chem. Soc.*, 2011, **133 (39)**, 15475.
17. L. E. Shea, *The Electrochemical Society Interface • Summer*, 1998, 24.
18. J. Ballato, J. S. Lewis and P. H. Holloway, *Mater. Res. Soc. Bull.*, 1999, **24**, 51.
19. H. C. Swart, T. A. Trottier, J. S. Sebastian, S. L. Jones and P. H. Holloway, *J. Appl. Phys.*, 1998, **83**, 4578.
20. S. S. Chadha, D. W. Smith, A. Vecht and C. Gibbons, *SID Dig.*, 1994, **25**, 51.
21. S. H. Cho, J. S. Yoo and J. D. Lee, *J. Electrochem. Soc.*, 1996, **143**, L231.
22. S. Itoh, H. Toki, K. Tamura, F. Kataoka and Jpn, *J. Appl. Phys.*, 1999, **31**, 6387.
23. C. W. Meyer, D. C. Meier, C. B. Montgomery, and S. Semancik, *Sens. Actuators, A*, 2006, **127**, 235.
24. M. D. Que, Z. P. Ci, Y. H. Wang, G. Zhu, B. T. Liu, J. Zhang, Y. R. Shi, Y. Wen, Y. Li, and Q. Wang, *J. Am. Ceram. Soc.*, 2012, 1.
25. G. Blasse, *Prog. Solid State Chem.*, 1988, **18**, 79.
26. J. Feng and H. J. Zhang, *Chem. Soc. Rev.*, 2013, **42**, 387.
27. G. J. Gao, S. Reibstein, M. Y. Peng and L. Wondraczek, *J. Mater. Chem.*, 2011, **21**, 3156.
28. G. J. Gao, J. X. Wei, Y. Shen, M. Y. Peng and L. Wondraczek, *Opt. Mater. Express*, 2014, **4**, 476.
29. G. Blasse, *J. Solid State Chem.*, 1975, **14**, 181.
30. M. Takahashi, K. Uematsu, Z. G. Ye and M. Sato, *Journal of Solid State Chemistry*, 1998, **139**, 304.
31. R. D. Shannon, *Acta Cryst.*, 1976, **A32**, 751
32. J. M. Phillips, et al, *Laser Photon. Rev.*, 2007, **1**, 307.
33. V. G. Zubkov, I. I. Leonidov, A. P. Tyutyunnik, N. V. Tarakina, I. V. Baklanova, L. A. Perelyaeva and L. L. Surat, *Physics of the Solid State*, 2008, **50**, 1699.
34. P. Kubelka, *J. Opt. Soc. Am.*, 1948, **38**, 448.
35. S. P. Tandon, J. P. Gupta, *Phys. Status Solidi B*, 1970, **38**, 363.
36. S. Fujihara, K. Tokumo, *Chem. Mater.*, 2005, **17**, 5587.

37. H. S. Yoo, W. B. Im, S. W. Kim, B. H. Kwon and D. Y. Jeon, *J. Lumin.*, 2010, **130**, 153.
38. G. J. Gao, J. X. Wei, Y. Shen, M. Y. Peng and L. Wondraczek, *J. Mater. Chem. C*, 2014, **2**, 8678.
39. G. J. Gao and L. Wondraczek, *J. Mater. Chem. C*, 2014, **2**, 691.
40. Y. Tian, B. J. Chen, R. N. Hua, N. S. Yu, B. Q. Liu, J. S. Sun, L. H. Cheng, H. Y. Zhong, X. P. Li, J. S. Zhang, B. N. Tian and H. Zhong, *Cryst Eng Comm.*, 2012, **14**, 1760.
41. R. A. Hansel, S. W. Allison and D. G. Walker, *Appl. Phys. Lett.*, 2009, **95**, 114102.
42. H. S. Jang, H. Y. Kim, Y. S. Kim, H. M. Lee and D. Y. Jeon, *Opt. Express*, 2012, **20**, 2761.
43. F. P. Du, Y. Nakai, T. Tsuboi, Y. Huang and H. J. Seo, *J. Mater. Chem.*, 2011, **21**, 4669.
44. Y. Tian, B. J. Chen, R. N. Hua, J. S. Sun, L. H. Cheng, H. Y. Zhong, X. P. Li, J. S. Zhang, Y. F. Zheng, T. T. Yu, L. B. Huang and H. Q. Yu, *J. Appl. Phys.*, 2011, **109**, 053511.
45. X. Liu, C. Li, Z. Quan, Z. Cheng and J. Lin, *J. Phys. Chem. C*, 2007, **111**, 16601.
46. X. M. Liu and J. Lin, *J. Mater. Chem.*, 2008, **18**, 221
47. Z. H. Xu, X. J. Kang, C. X. Li, Z. Y. Hou, C. M. Zhang, D. M. Yang, G. G. Li and J. Li, *Inorg. Chem.*, 2010, **49**, 6706.
48. Y. Zhang, G. G. Li, D. L. Geng, M. M. Shang, C. Peng and J. Lin, *Inorg. Chem.*, 2012, **51(21)**, 11655.
49. J. J. Hren, in *Principles of Analytical Electron Microscopy*, edited by D. C. Joy, A. D. Romig and J. I. Goldstein (Plenum, New York, 1986), 353.



The investigation on synthesis, structure and luminescence characteristics of a novel red phosphor NaLa₉(GeO₄)₆O₂:Eu³⁺ for LEDs and FEDs.